SENP1 promotes p27kip1 nuclear export though enhanced SUMOylation in cholangiocarcinoma leading to increased cell proliferation and chemoresistance

KAINIAN JIANG[1,2], WEI YANG[3], JIE HUANG[1,2], XIAOLONG TAN[1,2], YAN LIU[1,2], SAIYA TU[4] and JIAN LUO[1,2]

[1]Department of Geriatrics, Tongji Hospital, Tongji Medical College, Huazhong University of Science and Technology, Wuhan, Hubei 430030, P.R. China; [2]Key Laboratory of Vascular Aging, Ministry of Education, Tongji Hospital, Tongji Medical College, Huazhong University of Science and Technology, Wuhan, Hubei 430030, P.R. China; [3]Department of Hepatobiliary and Pancreatic Surgery, The Third People's Hospital of Hubei Province, Wuhan, Hubei 430030, P.R. China; [4]Second Clinical College, Tongji Medical College, Huazhong University of Science and Technology, Wuhan, Hubei 430030, P.R. China

Received November 5, 2024; Accepted June 5, 2025

DOI: 10.3892/ijmm.2025.5582

Abstract. SUMOylation is a critical post-translational modification, serving as a key role in nucleocytoplasmic translocation, transcriptional cofactor stabilization and modulation of chromatin remodeling factors, which are associated with oncogenesis, tumor progression and chemotherapy resistance in various types of cancer. SUMOylation was performed by small ubiquitin-like modifier (SUMO), a kind of small ubiquitin-like modifier, which was attached or removed from the substrates. The excessive export of nuclear p27kip1 induced by SUMOylation is associated with cell proliferation and chemotherapy resistance in cholangiocarcinoma (CCA). However, the exact underlying mechanism remains currently unknown. The present study investigated SUMO specific peptidase 1 (SENP1), which is known to participate in SUMOylation by activating nuclear SUMO1 precursors and deSUMOylating cytoplasmic substrates. SENP1 exhibited increased expression levels in CCA specimens compared with that in adjacent non-cancerous tissues, as confirmed by bioinformatics analysis and immunohistochemical assays. A significant correlation between SENP1 and p27kip1 expression levels was observed. SENP1 overexpression significantly increased cytoplasmic p27kip1 expression levels, thereby promoting CCA cell proliferation, accelerating the G_1-S cell cycle transition and reducing chemical sensitivity through increasing overall SUMOylation of p27kip1, as confirmed via western blotting, immunofluorescence, flow cytometry, Cell Counting Kit-8, 5-ethynyl-2'-deoxyuridine incorporation and SUMOylation tests. By contrast, SENP1 knockdown demonstrated the opposite results. Subsequently, the use of ML-792, COH000 and leptomycin B treatments, and the mutant variant SENP1-C603A demonstrated that SENP1 regulates the functionality of p27kip1 through nuclear SUMOylation rather than cytoplasmic deSUMOylation. The involvement of SENP1 represents a pivotal role in governing the nucleocytoplasmic shuttling of p27kip1. SENP1 knockdown could effectively impede CCA cell proliferation and enhance the chemosensitivity of cis-platinum by modulating the nuclear export of p27kip1 through SUMOylation, thus offering a potential therapeutic approach for CCA in the future.

Correspondence to: Professor Jian Luo, Department of Geriatrics, Tongji Hospital, Tongji Medical College, Huazhong University of Science and Technology, 1095 Jie Fang Avenue, Wuhan, Hubei 430030, P.R. China
E-mail: william76@163.com

Key words: small ubiquitin-like modifier specific peptidase 1, SUMOylation, p27kip1, cholangiocarcinoma, cell proliferation, cell cycle, chemoresistance

Introduction

Cholangiocarcinoma (CCA), a highly malignant and aggressive tumor derived from the biliary epithelium, exhibits an elevated incidence rate accounting for ~15% of all primary liver cancer cases and ~3% of gastrointestinal malignancies, and representing ~2% of all cancer-related deaths worldwide yearly, and demonstrates notable resistance to chemotherapy, while lacking effective clinical targets (1,2). CDK inhibitor 1B, also known as p27kip1, is a key CDK inhibitor that binds to CDK2-cyclin E1 within the nucleus, thereby inhibiting the transition of the cell cycle from G_1 to S phase (3,4). Cytoplasmic dislocation or abnormal expression levels of p27kip1 are associated with a poor clinical prognosis and drug resistance in certain cancer types, including lung, head and neck, colorectal and prostate (3,4). Additionally, p27kip1 serves a role in various cellular processes, such as cell proliferation, motility and apoptosis (5-7).

As a vital post-translational modification, small-ubiquitin-like modifiers (SUMOs) are covalently attached to their target proteins through a multi-step enzymatic cascade known as SUMOylation. SUMOylation and its inverse reaction,

deSUMOylation, serve important roles in regulating protein function by adding or removing SUMO proteins participating in diverse biological processes, such as nucleocytoplasmic translocation (8-10). SUMO-specific peptidases (SENPs) are key in activating SUMO precursors and dissociating SUMO substrate complexes (11,12).

Our previous study demonstrated that p27kip1 can be SUMOylated by SUMO1 and regulated by the only known SUMO E2 enzyme, ubiquitin conjugating enzyme E2 I (UBE2I), which is subsequently transported by chromosomal region maintenance 1 (CRM1) from the nucleus to the cytoplasm in CCA (13,14). However, the precise mechanism by which SENP1 regulates the SUMOylation and/or deSUMOylation of p27kip1, resulting in abnormal cytoplasmic localization, is currently unclear.

SENP1, a pivotal member of the SENP family, primarily localizes in the nucleus and functions as a specific protease for SUMO1. The start of the SUMOylation pathway is the activation of SUMO1 precursors by SENP1. The activated SUMO1 is then transferred to UBE2I. Ultimately, SUMO1 is covalently attached to lysine residues of substrates by SUMO E3 enzymes (8,9). The final step in SUMOylation involves the disassembly of SUMO1 from complexes with SUMO1-substrates by SENP1, which is thus also known as deSUMOylation (11,12). SENP1 undertakes two key functions in SUMO modification. The first function of SENP1 is to cleave the amino acids behind the Gly-Gly (GG) residues of SUMO1 C-terminal via hydrolase activity, which results in the maturation of SUMO1 precursors and the initiation of SUMO modification (15). The second function of SENP1 is to deconjugate SUMO1 from substrates though isopeptidase activity. However, the precise role of SENP1 in the distinct specific modification for various substrate proteins by selective SUMOylation and/or deSUMOylation remains controversial (8,9). Gao *et al* (16) reported that SENP1 promotes triple-negative breast cancer invasion and metastasis through GATA binding protein 1 deSUMOylation. Li *et al* (17) found that SENP1-mediated deSUMOylation of JAK2 regulates its kinase activity and platinum drug resistance. Furthermore, Zhu *et al* (18) reported that SENP1 promotes the development of Wilms' tumors by increasing the SUMOylation of hypoxia-inducible factor 1α.

Therefore, the present study aimed to investigate the correlation between SENP1 and p27kip1 in CCA and to elucidate the precise mechanism by which SENP1 regulates the SUMOylation and/or deSUMOylation process of p27kip1, resulting in its cytoplasmic accumulation through modulating p27kip1 nuclear export or disassembling cytoplasmic complexes of SUMO1-substrates.

Materials and methods

Patients, specimens and follow-up. In total, 36 patients with CCA (age range, 37-76 years) who underwent curative resection at the Pancreatobiliary Surgery Center of Tongji Hospital (Huazhong University of Science and Technology, Wuhan, China) between January 2016 and 2018 were enrolled in the present study. Patients were included if they did not receive chemotherapy before surgical resection, and all diagnoses were confirmed by the Department of Pathology of Tongji Hospital (Huazhong University of Science and Technology). CCA was staged according to the diagnostic criteria of the 8th edition of the American Joint Committee on Cancer staging system for biliary tract carcinoma (19). CCA tumor and paired adjacent non-cancerous tissues (ANT; 2 cm from the tumor) were collected for immunohistochemical (IHC) analyses. Complete clinicopathological data and follow-up results were collected for analysis. Patient follow-up lasted until October 2019. Overall survival was defined as the time interval between the date of surgery and the date of death or last follow-up. All study procedures were approved by the Ethics Committee of Tongji Hospital (approval no. TJ-IRB202502103) and conformed to the Declaration of Helsinki. Written informed consent was obtained from each patient.

Bioinformatics analysis of SENP1 expression levels and correlation with clinicopathological features of CCA using a pan-cancer database. The UALCAN (http://ualcan.path.uab.edu) portal was used to determine the expression profiles of SENP1 between tumor tissues and normal bile duct tissues from The Cancer Genome Atlas (TCGA; https://www.cancer.gov/ccg/research/genome-sequencing/tcga), and its impact on patient survival across 33 types of cancer. The differences in SENP1 expression were analyzed based on sample characteristics, such as individual cancer stage, tumor grade and lymph node metastasis status (20,21). The correlation between SENP1 and p27kip1 was analyzed by GEPIA2 (http://gepia2.cancer-pku.cn/) using Spearman's correlation analysis (22). The log-rank test was used to compare survival between groups. $P<0.05$ was considered to indicate a statistically significant difference.

IHC staining. From each patient, two sections were stained with the primary polyclonal antibody SENP1 (1:200; rabbit; cat. no. ab236094; Abcam) or monoclonal antibody p27kip1 (1:200; mouse; cat. no. 83630s; Cell Signaling Technology, Inc.), according to the standard procedure of the streptavidin-biotin complex method. Briefly, the tissues were paraffin-embedded, fixed with 10% neutral formalin at room temperature (RT) overnight and sectioned at 2 μm. The slices were dewaxed in xylene to water, incubated with 3% H_2O_2 for 10 min, washed with distilled water, soaked in PBS for 5 mins, blocked with 5% skimmed milk, incubated at RT for 10 min and incubated with anti-SENP1 antibody or anti-p27kip1 antibody overnight at 4°C. The next day, the sections were washed with PBS, incubated for 30 min at RT and washed again with PBS. A Dako EnVision kit (cat. no. K5007; Dako; Agilent Technologies, Inc.) was used for secondary antibody labeling and peroxidase activity detection. Secondary antibody (included in the kit) was incubated at RT for 30 min. The tissues were incubated with hematoxylin (Sigma-Aldrich; Merck KGaA) for 5 min at RT to counterstain the nuclei. The IHC stained sections were analyzed blindly by two independent pathologists via light microscopy. The membrane staining of each section was examined and semi-quantitatively scored according to each histological component using the immune response scoring system (IRS) (23). The IRS was defined as the product of the percentage of positive cells (0, none; 1, ≤10%; 2, 10-50%; 3, 51-80%; and 4 ≥80%) and the estimated intensity (0, negative; 1, weak; 2, medium; and 3, strong). The final IRS values were

between 0 and 12. An IRS score of >4 was considered to indicate a positive expression, while ≤4 was considered to indicate negative expression for SENP1.

Cell culture. The TFK1, HuCCT1 and 293T cells were purchased from The Cell Bank of Type Culture Collection of The Chinese Academy of Sciences. RBE cells were purchased from Wuhan Warner Biotechnology Co., Ltd. TFK1 and 293T cells were maintained in Dulbecco's modified Eagle's medium (DMEM; HyClone; Cytiva) supplemented with 10% fetal bovine serum (Shanghai Nova Pharmaceutical Technology Co., Ltd.), 100 μg/ml streptomycin and 100 U/ml penicillin (Beijing Solarbio Science & Technology Co., Ltd.) in a humidified atmosphere with 5% CO_2 at 37˚C. HuCCT1 and RBE cells were maintained in RPMI 1640 medium (HyClone; Cytiva) supplemented with 10% fetal bovine serum (Shanghai Nova Pharmaceutical Technology Co., Ltd.), 100 μg/ml streptomycin and 100 U/ml penicillin (Beijing Solarbio Science & Technology Co., Ltd.) in a humidified atmosphere with 5% CO_2 at 37˚C.

Transient siRNA transfection. RBE and TFK1 cells were transfected with siRNA using Lipofectamine™ 3000 (Thermo Fisher Scientific, Inc.) according to the manufacturer's instructions. The cells were transfected with 20 nM siRNA in a humidified atmosphere with 5% CO_2 at 37˚C for 8 h. The time interval was 48 h between transfection and subsequent experimentations. The siRNAs for SENP1 were bought from Beijing Augct DNA-Syn Biotechnology Co., Ltd. The siRNA sequences were as follows: siSENP1-1 sense, 5'-GGAAAU GGAGAAAGAAAUATT-3' and antisense, 3'-UAUUUCUUU CUCCAUUUCCTT-5'; siSENP1-2 sense, 5'-GGAAAGAGU UUGACACCAATT-3' and antisense, 3'-UUGGUGUCAAAC UCUUUCCTT-5'; and siSENP1-3 sense, 5'-AGAAGAAGA AAGAGAGAUUTT-3' and antisense, 3'-AAUCUCUCUUUC UUCUUCUTT-5'. The negative control siRNA sense was 5'-UUGUACUACACAAAAGUACUGTT-3' and the antisense was 3'-CAGUACUUUUGUGUAGUACAA-5'. The siGAPDH sense was 5'-GUAUGACAACAGCCUCAAGTT-3' and the antisense was 3'-CUUGAGGCUGUUGUCAUACTT-5'.

Lentivirus production, transfection and establishment of stable cell clones. The lentivirus construction was generated using a 2nd generation system. The control vector pLVX-puro, SENP1 overexpression and SENP1 C603A mutation plasmid were attached with the FLAG-tag and purchased from Beijing Augct DNA-Syn Biotechnology Co., Ltd. The psPAX2 (cat. no. #12260) and pMD2.G (cat. no #12259) packaging plasmids were purchased from Addgene, Inc. A total of 4 μg SENP1 overexpression and C603A mutation plasmids, as well as their control, vector pLVX-puro, were separately transfected into 293T cells with 3 μg psPAX2 and 3 μg pMD2.G using Lipofectamine™ 3000 Transfection Reagent (Thermo Fisher Scientific, Inc.) in a 60-mm cell culture dish. After 48 h of incubation, the virus-containing supernatant was collected and filtered through a 0.22-μm filter. CCA cell lines RBE and TFK1 were transfected with lentiviral particles in the presence of 8 μg/ml polybrene (Calbiochem; Merck KGaA) at 37˚C with a multiplicity of infection ranging from 20 to 100. Next, 72 h after transfection, the cells were selected for 2 weeks using 2 μg/ml puromycin (Calbiochem; Merck KGaA) for RBE cells and 4 μg/ml puromycin for TFK1 cells. The cells were then cultured with the maintenance concentration 1 μg/ml puromycin for RBE cells and 2 μg/ml puromycin for TFK1 cells. There was 48 h between selection and subsequent experimentation with the cells.

Cell protein isolation and western blot. CCA cell line RBE and TFK1 were lysed with RIPA buffer (Wuhan Boster Biological Technology, Ltd.) added with proteinase and phosphatase inhibitor cocktail (Roche Diagnostics) for western blotting or immunoprecipitation (IP) buffer (cat. no. G2038; Wuhan Servicebio Technology Co., Ltd.) supplemented with protease inhibitors (for SUMOylation assay) for 1 h on ice. The protein concentration was determined using Pierce™ BCA Protein Assay Kits (Thermo Fisher Scientific, Inc.). In each lane, 20 μg protein from each sample was separated by 10 or 12% SDS-PAGE (Wuhan Boster Biological Technology, Ltd.) and transferred to a polyvinylidene difluoride membrane (MilliporeSigma). The membrane was blocked with 5% skimmed milk dissolved by 1X Tris-buffered saline containing 0.1% Tween-20 at RT for 1 h. Then, the membranes were incubated with primary antibodies against SENP1 (cat. no. 25349-1-AP; 1:1,000; Proteintech Group, Inc.), Lamin B1 (cat. no. 66095-1-Ig; 1:10,000; Proteintech Group, Inc.), β-tubulin (cat. no. 66240-1-Ig; 1:20,000; Proteintech Group, Inc.), GAPDH (cat. no. 60004-1-Ig; 1:20,000, Proteintech Group, Inc.), p27kip1 (cat. no. #3686S; 1:1,000; Cell Signaling Technology, Inc.), cyclin D1 (cat. no. #55506S; 1:1,000; Cell Signaling Technology, Inc.), cyclin E1 (cat. no. #20808S; 1:1,000; Cell Signaling Technology, Inc.), CDK2 (cat. no. #18048S; 1:1,000; Cell Signaling Technology, Inc.), Bcl-2 (cat. no. #4223S; 1:1,000; Cell Signaling Technology, Inc.), cleaved caspase-3 (cat. no. #9661S; 1:1,000; Cell Signaling Technology, Inc.), caspase-3 (cat. no. 19677-1-AP; 1:1,000; Proteintech Group, Inc.), Bax (cat. no. #5023; 1:1,000; Cell Signaling Technology, Inc.), multidrug resistance 1 (MDR1; cat. no. #13342; 1:1,000; Cell Signaling Technology, Inc.) and multidrug resistance-associated protein 1 (MRP1; cat. no. #14685; 1:1,000; Cell Signaling Technology, Inc.) at 4˚C overnight. Subsequently, the membranes were incubated with HRP-conjugated anti-rabbit (cat. no. 33101ES60, 1:5,000; Shanghai Yeasen Biotechnology Co., Ltd.) or -mouse (cat. no. 33201ES60, 1:5,000; Shanghai Yeasen Biotechnology Co., Ltd.) secondary antibodies at 37˚C for 2 h. Detection was performed using a ChemiDoc™ Imaging System (Bio-Rad Laboratories, Inc.). Nuclear and cytoplasmic proteins were separated using the Nuclear and Cytoplasmic Protein Extraction Kit (cat. no. 20126ES60; Shanghai Yeasen Biotechnology Co., Ltd.), following the manufacturer's instructions.

Co-IP assays. RBE and TFK1 cells were cultured in a 60-mm culture dish after lentivirus or siRNA transfection and lysed with 500 μl IP buffer (cat. no. G2038; Wuhan Servicebio Technology Co., Ltd.) supplemented with protease inhibitors. The buffer was then centrifuged at 13,000 x g for 20 min at 4˚C. The protein concentration was determined using Pierce™ BCA Protein Assay Kits (Thermo Fisher Scientific, Inc.). Overall, 1,000 μg total protein was incubated with 2 μg SENP1 antibody (cat. no. 25349-1-AP; Proteintech Group,

Inc.) or p27kip1 antibody (cat. no. #3686S; Cell Signaling Technology, Inc) separately and oscillated for 4 h at 4˚C. For each reaction, 40 μl protein A/G magnetic beads (cat. no. B23201; Bimake) were added and the mixture were oscillated overnight at 4˚C. The beads were washed three times with IP wash buffer [50 mM Tris-Cl, 1 mM EDTA (pH 7.5), 1% NP-40 and 300 mM NaCl] and eluted with 1X loading buffer or elution buffer from Universal IP/Co-IP Toolkit (Magnetic Beads) (cat. no. KTD104; Abbkine Scientific Co., Ltd.) to maintain the conjugation of the proteins. The beads were isolated by magnetic frame. Eluted proteins by loading buffer were heated at 100˚C for 5 min, and the bound proteins were further analyzed by western blot analysis.

Immunofluorescence. RBE CCA cells were seeded on coverslips and cultured for 8 h. Subsequently, the cells were washed with PBS and then fixed with 4% paraformaldehyde for 15 min at RT. After rinsing with PBS, cells were permeabilized and blocked with 0.5% Triton-100 and 5% goat serum (cat. no. G1208-5ML; Wuhan Servicebio Technology Co., Ltd.) in PBS for 1 h at RT. Coverslips with cells were then incubated with primary antibodies (diluted in blocking buffer) overnight at 4˚C, followed by incubation with secondary antibodies conjugated with YSFluor® 488 (cat. no. 33106ES60, 1:200; Shanghai Yeasen Biotechnology Co., Ltd.) or YSFluor 594 (cat. no. 33112ES60, 1:200; Shanghai Yeasen Biotechnology Co., Ltd.) in the dark at RT for 1 h. Primary antibodies included anti-p27kip1 (cat. no. #3686S; 1:100; Cell Signaling Technology, Inc.) and anti-SENP1 (cat. no. ab108981; 1:100; Abcam). Next, cells were washed and stained using DAPI (cat. no. 40728ES03, 3 μg/ml; Shanghai Yeasen Biotechnology Co., Ltd.) on the coverslips for 5 min, after which coverslips were washed with PBS for 3 times. Then the coverslips were covered on the microslides. Cells were visualized and images captured using a confocal microscope (Nikon Corporation).

SUMOylation assay. The p27kip1 SUMOylation levels were detected by the EpiQuik *in vivo* Protein SUMOylation Assay Ultra Kit (EpigenTek Group, Inc.) according to the manufacturer's protocol. Briefly, the cell extracts were immunoprecipitated with anti-p27kip1 antibody followed by anti-SUMO1 antibody.

Flow cytometry. RBE and TFK1 cell (negative control, SENP1 overexpression and siSENP1 groups treated with cis-platinum for 12 h) apoptosis was analyzed by flow cytometry using FITC Annexin V Apoptosis Detection Kit I (BD Biosciences) according to the manufacturer's instructions. The cells and the medium were collected and centrifuged at 179 x g at RT for 10 min, washed with precooled PBS and centrifuged at 179 x g at RT for 10 min again. Subsequently, the samples were resuspended with 300 μl 1X Binding Buffer and incubated with 5 μl Annexin V-FITC in the dark at RT for 15 min, before adding 5 μl PI and 200 μl 1X Binding Buffer before analyzation. The PI/RNase Staining buffer (BD Biosciences) was used for analyzing the cell cycle of the RBE and TFK1 cells (negative control, SENP1 overexpression and siSENP1 groups) according to the manufacturer's instructions. The cells were collected and centrifuged at 1,000 x g at 4˚C for 5 min and then were resuspended with 1 ml precooled PBS, after which 3 ml ethyl alcohol was added at 4˚C overnight to fix the cells. The fixed cells were centrifuged at 1,000 x g at 4˚C for 5 min, washed with 1 ml precooled PBS and centrifuged at 1,000 x g at 4˚C for 5 min again. Subsequently, the cells were resuspended with 0.5 ml PI/RNase, incubated in the dark at RT for 30 min and filtered with 300-mesh nylon mesh. The results were analyzed with the flow cytometer (FACSCalibur™; BD Biosciences) and the FlowJo software (BD Biosciences).

IC_{50} calculation of cis-platinum. The RBE and TFK1 (negative control, SENP1 overexpression and siSENP1 groups) cells were seeded at a density of ~$5x10^4$ cells in a 96-well plate and incubated for 8 h in 100 μl of medium (DMEM for TFK1 and RPMI 1640 for RBE) supplemented with 10% FBS. Subsequently, the medium was replaced with a concentration ladder ranging from 1 to 100 μM for cis-platinum (MedChemExpress). After further incubation for 12 h, Cell Counting Kit-8 reagent (cat. no. HY-K0301; MedChemExpress) was added and incubated at 37˚C for 1 h to assess cell viability. The optical density was measured at a wavelength of 450 nm using a microplate reader (cat. no. Elx800; Omega Bio-Tek, Inc.). Data analysis was performed using GraphPad Prism (version 8.0; Dotmatics).

Cell proliferation assay. The cells were seeded at a density of $1x10^3$ cells per well in 96-well plates containing 100 μl DMEM or RPMI 1640 medium supplemented with 10% FBS. At the designated time points, Cell Counting Kit-8 reagent (cat. no. HY-K0301; MedChemExpress) was added and incubated for 1 h at 37˚C. The absorbance at a wavelength of 450 nm was measured using a microplate reader (cat. no. Elx800; Omega Bio-Tek).

DNA synthesis via 5-ethynyl-2'-deoxyuridine (EdU) incorporation assays. The proliferation rate of cells was determined using a Yefluor488EdU Imaging kit (cat. no. 40275ES76; Shanghai Yeasen Biotechnology Co., Ltd.) (https://www.yeasen.com/products/detail/1569). Briefly, 50,000 cells per well of transfected cells were plated in 24-well plates. At 24 h post-seeding, cells were incubated with 10 nM EdU 2 h, before fixation with 4% PFA at RT for 2 h and EdU incorporation determined by staining using the Yefluor488EdU Imaging kit according to the manufacturer's instructions. Nuclei were counterstained with Hoechst 33342 (included in the Yeflour 488 EdU Imaging kit) in the dark at RT for 30 min. Images were captured using an fluorescence inverted microscope.

ML-792, COH000 and leptomycin B (LMB) treatments. For nuclear export inhibition assays, cells were treated with 20 nM LMB (Beyotime Institute of Biotechnology), to block the p27kip1 transporter CRM1, at 37˚C for 12 h in 10% FBS in medium, which was then used for nuclear and cytoplasmic protein separation, WB and SUMOylation tests. ML-792 and COH000 were inhibitors of SUMOylation E1 and were used to mimic the inhibition of SENP1 hydrolase activity. Treatment with 1 μM ML-792 (MedChemExpress) and 0.2 μM COH000 (MedChemExpress) were performed at 37˚C for 12 h for SUMOylation inhibition. The cells were subsequently used for nuclear and cytoplasmic protein separation, WB and SUMOylation tests.

Statistical analysis. Data are expressed as the mean ± SEM from experiments performed in triplicate. Statistical analysis was performed using GraphPad Prism (version 8.0; Dotmatics) software. Comparisons between two groups were analyzed using two-tailed unpaired Student's t-tests for normally distributed data. The paired data from the samples of tumor tissue and adjacent non-tumor tissue from the same patient were analyzed using the Wilcoxon signed rank test. Fisher's exact test was performed to analyze the associations between SENP1 expression levels and clinicopathological characteristics of CCA. Comparisons of multiple groups were performed by one-way analysis of variance with Bonferroni's post hoc test (parametric). $P<0.05$ was considered to indicate a statistically significant difference.

Results

SENP1 expression is associated with clinicopathological characteristics and prognosis in CCA. Analysis using the UALCAN portal of TCGA data across a pan-cancer panel demonstrated that SENP1 expression levels were significantly increased in 18 out of 33 types of cancer compared with that of normal samples, suggesting that upregulation of SENP1 serves a pivotal role in tumorigenesis (Fig. 1A). Within the CCA group (n=36), notable differences were observed compared with the normal tissue sample group (n=9), particularly among the 18 types of tumors exhibiting increased SENP1 expression (Fig. 1B). The increased expression levels of SENP1 demonstrated significant associations with tumor stage and lymph node metastasis; however, significant differences only occurred in comparisons between the normal bile duct tissues and tissues from each tumor stage (Fig. 1B; Table I). There were no significant differences in the SENP1 expression levels when comparing the samples from different tumors and lymph node metastasis stages of CCA. The upregulated expression levels of SENP1 were closely associated with CCA tumorigenesis (Fig. 1B). However, no correlation was observed with reduced patient survival status according to the UALCAN web portal (Fig. 1B).

To further determine the clinical significance of SENP1 in CCA development, 36 CCA and paired ANT samples from surgical patients were collected. Consistent with the findings from TCGA data, SENP1 expression levels in CCA tissues were significantly increased compared with those of ANT samples (6.91±0.57 vs. 4.86±0.45; Fig. 1C). Increased SENP1 expression levels were closely associated with advanced TNM [TNM I-II vs. TNM III-IV, 50 (10/20) vs. 87.50% (14/16)] and lymph node metastasis [absent vs. present, 47.06 (8/17) vs. 84.21% (16/19)], showing significant associations using IHC staining (Table II). There were no statistically significant differences observed in terms of age, sex, serum CA19-9 levels, differentiation degree, vascular invasion local invasion, stage and survival (Table II). Additionally, correlation analysis demonstrated a significant positive association between SENP1 and p27kip1 mRNA expression levels in CCA tissues by GEPIA2 (Fig. 1D) (22). Notably increased p27kip1 expression shifting from nuclear to cytoplasm localization, with the progression of TNM stages from I-II to III-IV was observed (Fig. 1E). Consequently, it could be considered that the positive correlation might be more contingent upon the interplay between SENP1 and p27kip1 in the cytoplasm. SENP1 could be a potential diagnostic marker.

Table I. Statistical comparisons of The Cancer Genome Atlas cholangiocarcinoma data.

Comparison	P-value
Normal vs. primary	1.63×10^{-12}
Normal vs. stage 1	1.67×10^{-8}
Normal vs. stage 2	1.24×10^{-4}
Normal vs. stage 3	N/A
Normal vs. stage 4	4.70×10^{-3}
Stage 1 vs. stage 2	0.64
Stage 1 vs. stage 3	N/A
Stage 1 vs. stage 4	0.45
Stage 2 vs. stage 3	N/A
Stage 2 vs. stage 4	0.32
Stage 3 vs. stage 4	N/A
Normal vs. N0	2.36×10^{-11}
Normal vs. N1	7.64×10^{-3}
N0 vs. N1	0.72

N/A, not applicable.

SENP1 facilitates nuclear export of p27kip1 by promoting p27kip1 SUMOylation in CCA. SENP1 serves a key role in SUMOylation, participating in nucleocytoplasmic translocation (24). The effects of SENP1 on p27kip1, particularly its subcellular distribution and SUMO modification, were investigated in the present study. First, the subcellular localization and expression levels of SENP1 in CCA cell lines (RBE, TFK1 and HuCCT1) were examined using immunofluorescence and western blotting. Predominantly nuclear localization of SENP1 with limited cytoplasmic presence in all CCA cell lines (Fig. 2A) was observed. siRNAs specifically targeting SENP1 were designed and transfected into the RBE extrahepatic CCA cell line (Fig. 2B). Among the various siRNAs, siSENP1-3 was chosen for further examination as it showed the most efficient silencing (Fig. 2B). Additionally, overexpression of SENP1 was achieved in the RBE cell line using a lentivirus to generate SENP1-overexpression (SENP1-oe) cells (Fig. 2C). SENP1-oe and siSENP1 cells did not show altered cellular distribution of SENP1 (Fig. 2D and E). The precise effects of SENP1 on p27kip1 were unknown, therefore p27kip1 expression levels were examined using western blot in siSENP1 and SENP1-oe cells. p27kip1 expression levels were not significantly altered by SENP1-oe or knockdown (Fig. 2B and C). It could be inferred that SENP1 might not affect the synthesis or degradation of p27kip1.

Subsequently, co-IP assays were used to determine the interactions between SENP1 and p27kip1. Co-IP demonstrated the direct interaction of SENP1 and p27kip1 (Fig. 3A). The overall SUMOylation levels of the p27kip1 protein were analyzed in RBE cells. Overexpression of SENP1 significantly increased the total SUMOylation of p27kip1 in SENP1-oe cells compared with that in VEC cells, which was associated with a notable

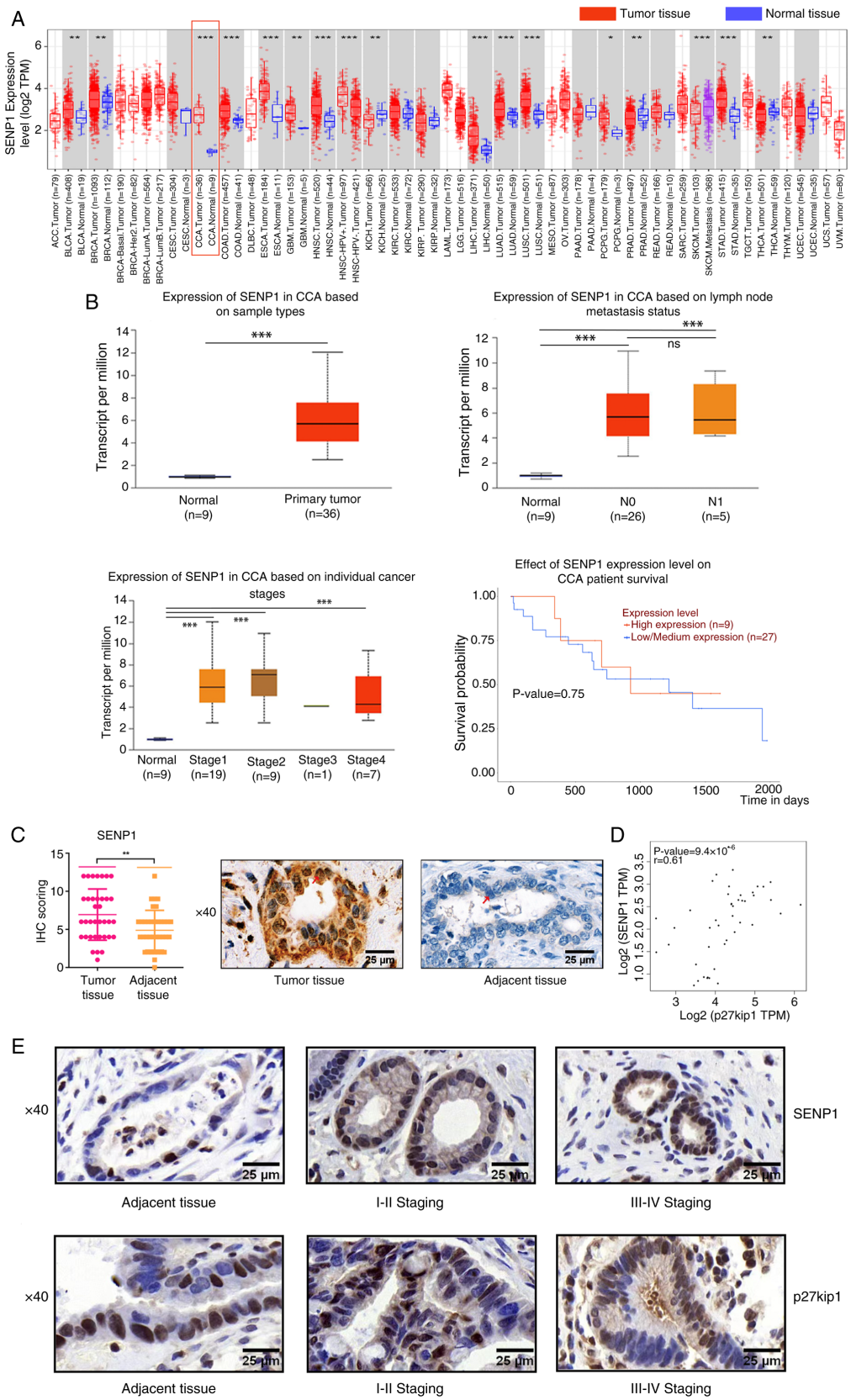

Figure 1. Analysis of TCGA data and clinical samples demonstrating the gene and protein SENP1 expression levels in CCA tissues compared with that in normal tissue samples. (A) Analysis of TCGA data demonstrated increased SENP1 gene expression in numerous types of cancer evaluated using the UALCAN software. The red box indicates the CCA data. (B) TCGA data analysis showed increased gene expression levels of SENP1 CCA, which were associated with lymph node metastasis and tumor stage, evaluated using the UALCAN software. (C) IHC analysis demonstrated increased SENP1 protein expression levels in the CCA cells compared with those of adjacent healthy tissues. The red arrows indicate nuclei with a different expression level of SENP1. Scale bar, 25 μm; magnification, x40. (D) Correlation analysis demonstrated a significant positive association between SENP1 and p27kip1 expression levels in CCA tissues using GEPIA 2 analysis (r=0.61; P<0.01). (E) IHC analysis demonstrated that the expression of SENP1 and the cytoplasmic p27kip1 localization increase with increasing CCA tumor stages. Error bar, mean ± SEM; scale bar, 25 μm; magnification, x40. *P<0.05, **P<0.01 and ***P<0.001. ns, not significant; CCA, cholangiocarcinoma; SENP1, SUMO specific peptidase 1; TCGA, The Cancer Genome Atlas; TPM, transcripts per million; IHC, immunohistochemical.

Table II. Association of SENP1 expression with clinicopathological characteristics of patients with cholangiocarcinoma.

Clinicopathological data	No. of cases	Positive expression of SENP1 (n=24)	Negative expression of SENP1 (n=12)	P-value[a]
Age, years				0.720
≤60	23	16	7	
>60	13	8	5	
Sex				0.730
Male	20	14	6	
Female	16	10	6	
CA19-9, U/ml				>0.999
≤40	12	8	4	
>40	24	16	8	
Vascular invasion				>0.999
Unidentified	33	22	11	
Identified	3	2	1	
Local invasion				0.298
Unidentified	16	9	7	
Identified	20	15	5	
Lymph node metastasis				0.033
Absent	17	8	9	
Present	19	16	3	
TNM staging				0.032
I-II	20	10	10	
III-IV	16	14	2	
Differentiation degree				>0.999
Low or medium differentiation	29	19	10	
High differentiation	7	5	2	

[a]Fisher's exact test. SENP1, SUMO specific peptidase 1.

increase in p27kip1 cytoplasmic accumulation and reduction of p27kip1 nuclear levels (Fig. 3B-D). SENP1-oe RBE cells were used to demonstrate p27kip1 time-dependent translocation and SUMOylation. Translocation and SUMOylation p27kip1 levels were highest at 40 h (Fig. 3E and F). By contrast, the knockdown of SENP1 reduced the overall SUMOylation of p27kip1 compared with that of negative control cells (Fig. 3G). SENP1 knockdown was associated with a significant increase in the protein expression levels of nuclear p27kip1 and a decline in cytoplasmic p27kip1, characterized by the nuclear retention of p27kip1 in RBE cells (Fig. 3H and I). The time-dependent assay also showed the highest levels of translocation occurred after 40 h post-transfection and highest levels of SUMOylation of p27kip1 occurred at 32 h post-transfection (Fig. 3J and K). These findings suggested that SENP1 determines the overall SUMOylation level and nucleocytoplasmic shuttling of p27kip1 in CCA cells. SENP1 served a crucial role in regulating the nucleocytoplasmic shuttling of p27kip1 through SUMOylation involvement.

To further clarify whether nucleocytoplasmic shuttling of p27kip1 induced by SENP1 is attributed to nuclear export of p27kip1, LMB, a specific inhibitor of CRM1 (the transporter of p27kip1 across nucleus and cytoplasm), was used to specifically inhibit the nuclear export of p27kip1 involved in nuclear SUMOylation (14,25,26). The LMB treatment significantly increased p27kip1 nuclear retention in SENP1-oe and VEC RBE cells, accompanied by a corresponding increase in SUMOylation of p27kip1 in SENP1-oe cells within the nucleus. However, p27kip1 expression levels in the cytoplasm showed no significant increase (Fig. 4A and B). Nuclear SUMOylated p27kip1 expression levels of siSENP1 cells treated with LMB were also examined, which showed the same nuclear retention of p27kip1 but reduction of SUMOylated p27kip1 expression levels within the nucleus, showing the inverse results compared with that of SENP1-oe cells (Fig. 4C and D). This suggested that SENP1 facilitates p27kip1 SUMOylation and promotes nuclear export, resulting in p27kip1 cytoplasmic accumulation.

SENP1 serves a minor role in the deSUMOylation of p27kip1 in the cytoplasm in CCA. SENP1 serves a pivotal dual role in the SUMOylation and deSUMOylation, relying on the two enzymatic activities of SENP1: Isopeptidase and hydrolase. The hydrolase activity processes SUMO1 precursor maturation through the cleavage of its amino acid residues following the GG sequence, activated by the E1 enzyme, resulting in nuclear SUMOylation (8). Additionally, the isopeptidase

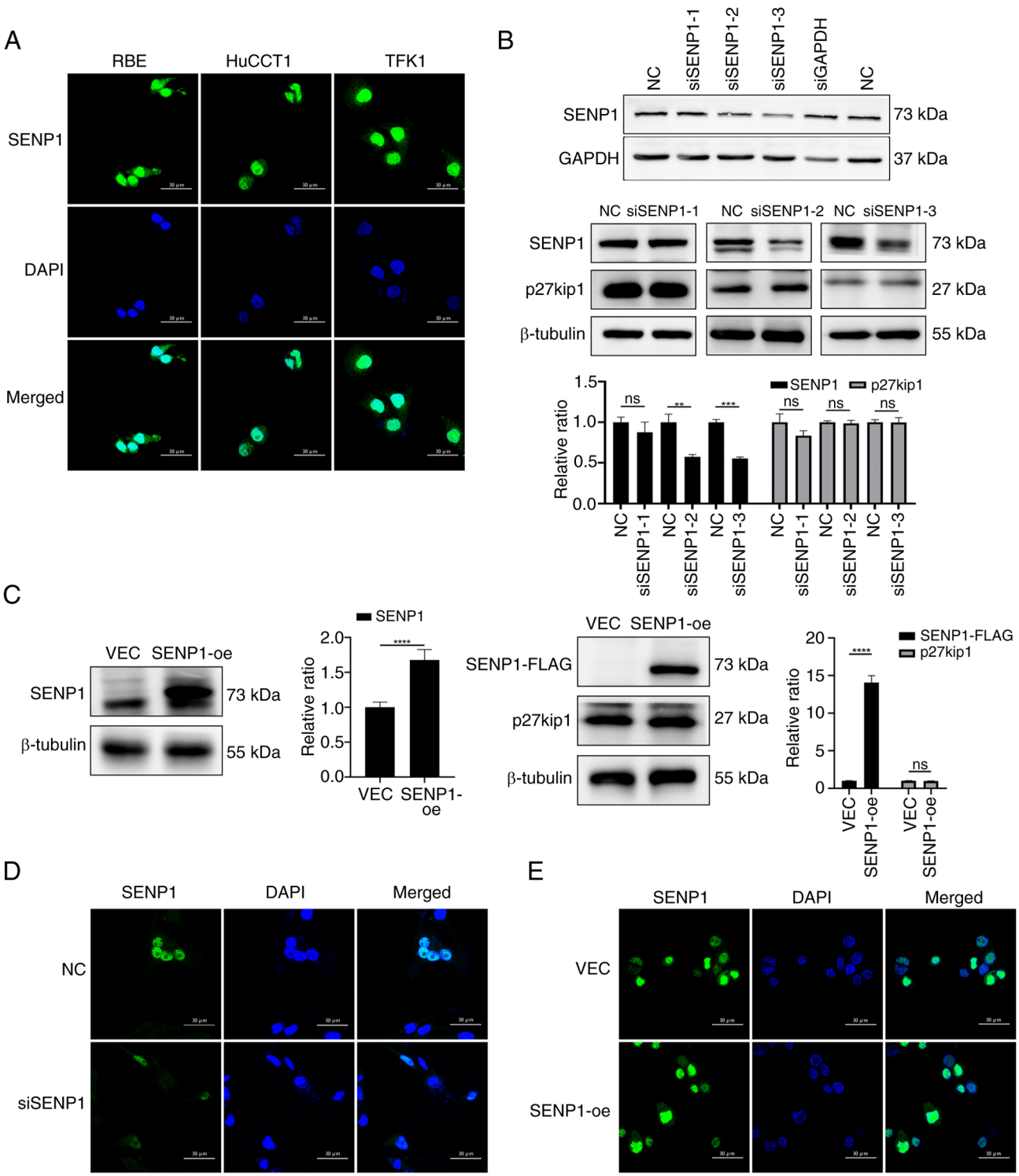

Figure 2. SENP1 knockdown or overexpression in CCA cell lines. SENP1 knockdown or overexpression did not affect localization or expression levels of p27kip1. (A) Localization of SENP1 in RBE, HuCCT1 and TFK1 CCA cell lines. Immunofluorescence assays showed predominant nuclear localization of SENP1 with limited cytoplasmic presence in all CCA cell lines. (B) Western blotting demonstrated the effect of siSENP1 1-3 in the RBE cell line; SENP1 knockdown did not affect p27kip1 expression levels (siGAPDH was used as the positive control to confirm that the transfection reagent was effective). (C) Western blotting demonstrated the effects of SENP1-oe in the RBE cell line; SENP1-oe did not affect p27kip1 expression levels. (D) Subcellular localization of SENP1 is unaffected in siSENP1 cells, compared with that in VEC cells. (E) Subcellular localization of SENP1 is unaffected in SENP1-oe cells, compared with that in VEC cells. Error bar, mean ± SEM; scale bar, 30 μm; magnification, x100. **P<0.01, ***P<0.001 and ****P<0.0001. CCA, cholangiocarcinoma; SENP1, SUMO specific peptidase 1; NC, negative control; VEC, empty vector lentivirus; si, small interfering; oe, overexpression.

activity deconjugates SUMO1 from the target protein lysine, leading to cytoplasmic deSUMOylation (Fig. 5A). However, the exact regulatory mechanism underlying the impact of SENP1 on p27kip1 is currently unclear.

ML-792 and COH000, the SUMOylation inhibitors, were used to mimic the suppression of SENP1-mediated hydrolase activity in the nucleus (27). SENP1 knockdown, and ML-792 and COH000 treatments were associated with

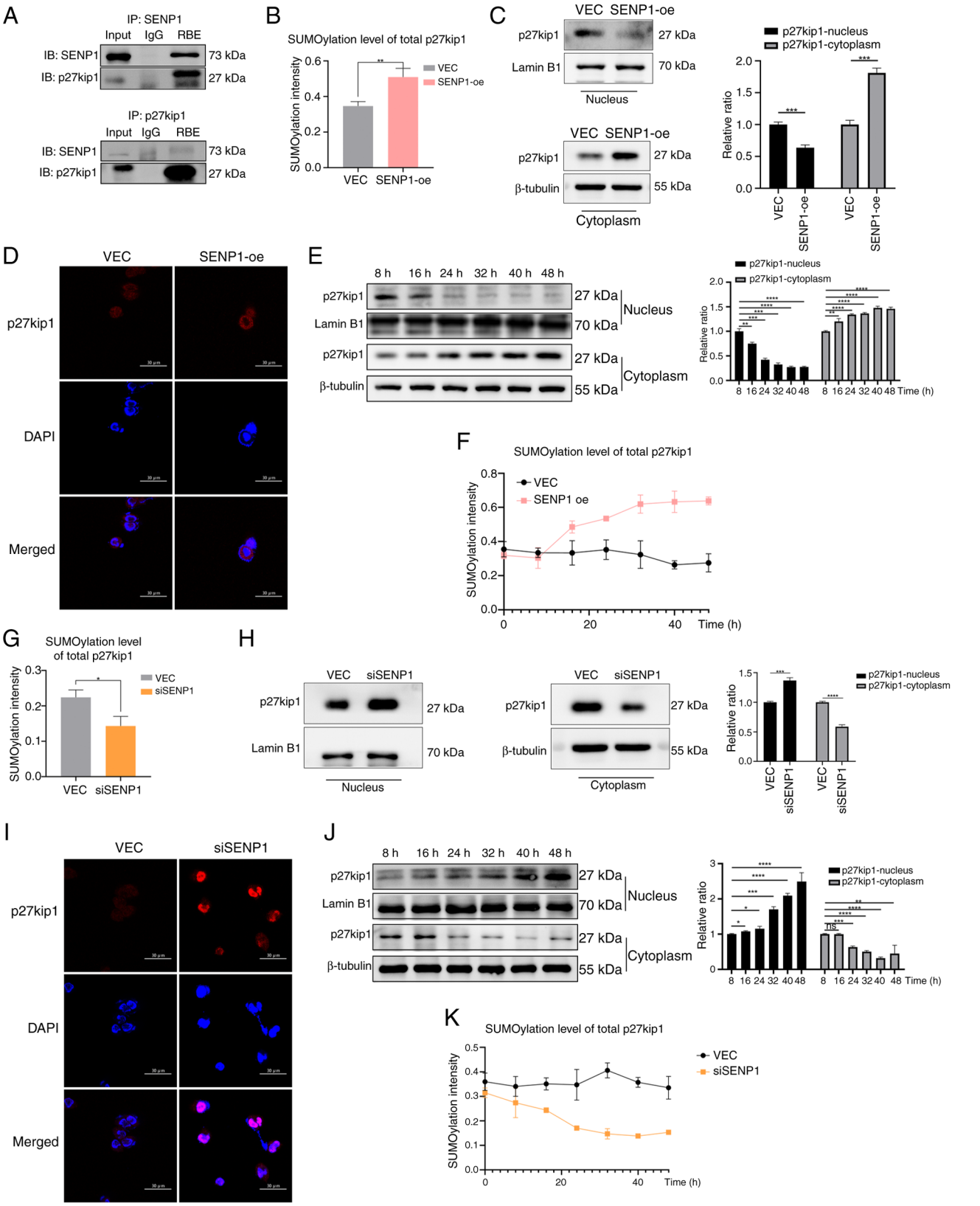

Figure 3. SENP1 influences p27kip1 SUMOylation and subcellular localization. (A) Interactions between p27kip1 and SENP1 co-IP assay demonstrated using co-IP assays. (B) SENP1-oe promoted the SUMOylation of p27kip1 in RBE cells. (C) Western blotting and the nuclear and cytoplasmic proteins isolation assays showed the increased nuclear p27kip1 and decreased cytoplasmic p27kip1 expression levels in the RBE cells. (D) Immunofluorescence showed increased nuclear p27kip1 and decreased cytoplasmic p27kip1 levels in the RBE cells. (E) Time-dependent p27kip1 expression levels in the nucleus and cytoplasm within SENP1-oe cells. (F) Time-dependent p27kip1 SUMOylation levels within SENP1-oe cells. (G) Transfection with siSENP1 reduced the SUMOylation of total p27kip1 in the RBE cells. (H) Western blotting and the nuclear and cytoplasmic proteins isolation assays showed the reduction of nuclear p27kip1 and increase of cytoplasmic p27kip1 in the RBE cells. (I) Immunofluorescence assay showed decreased nuclear p27kip1 and increased cytoplasmic p27kip1 levels in the RBE cells. (J) Time-dependent p27kip1 expression levels in the nucleus and cytoplasm. (K) Time-dependent SUMOylation levels of p27kip1 following SENP1 transfection. Error bar, mean ± SEM; scale bar, 30 μm; magnification, x100. *P<0.05, **P<0.01, ***P<0.001 and ****P<0.0001. SENP1, SUMO specific peptidase 1; NC, negative control; VEC, empty vector lentivirus; si, small interfering; oe, overexpression; IP, immunoprecipitation.

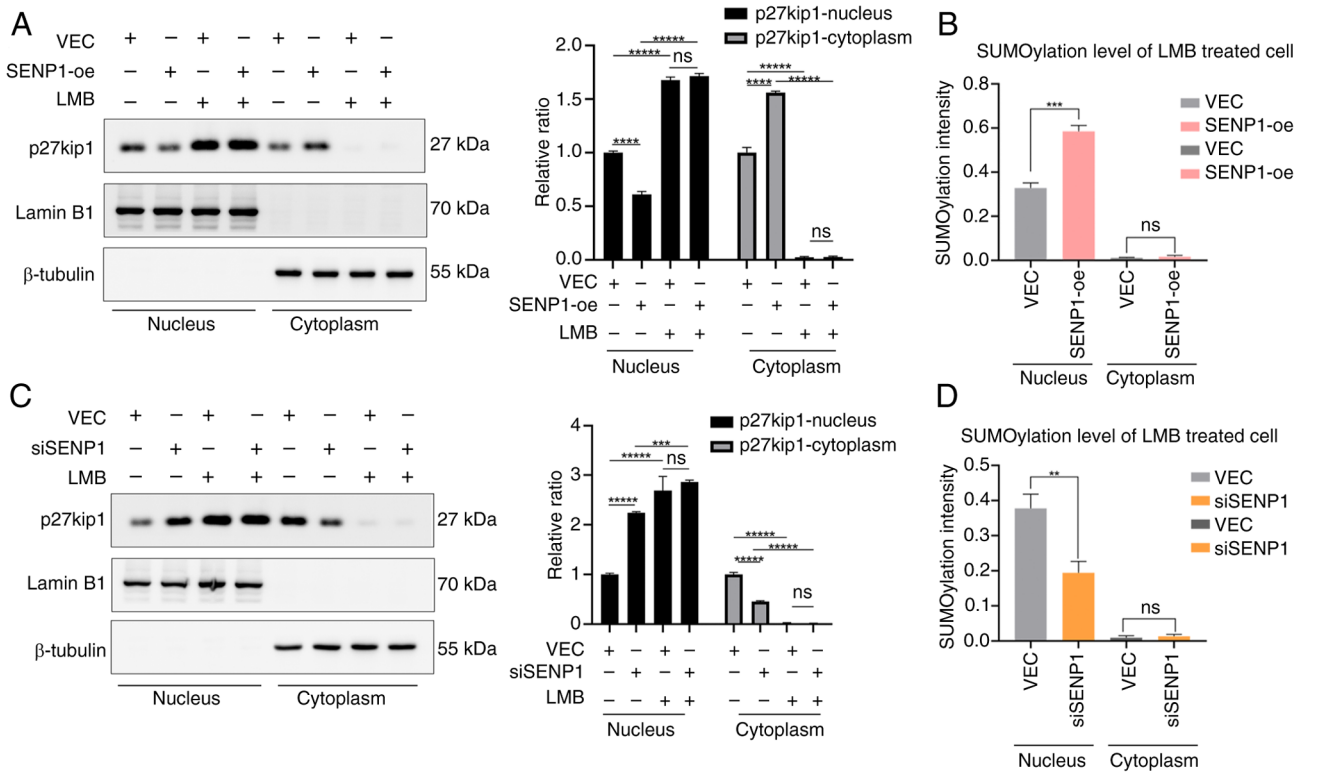

Figure 4. SUMOylation levels of nuclear and cytoplasmic p27kip1 in LMB-treated cells. (A) LMB treatment restricted the p27kip1 inside the nucleus of SENP1-oe RBE cells. (B) LMB-treated RBE cells showed significantly increased levels of nuclear SUMOylated p27kip1, but no significant changes in cytoplasmic SUMOylated p27kip1 expression levels. (C) LMB treatment restricted the p27kip1 inside the nucleus of siSENP1 RBE cells. (D) LMB-treated siSENP1 RBE cells showed significantly decreased levels of nuclear SUMOylated p27kip1, but no significant changes in cytoplasmic SUMOylated p27kip1 expression levels. Error bar, mean ± SEM. **P<0.01, ***P<0.001, ****P<0.0001 and *****P<0.00001. ns, not significant; SENP1, SUMO specific peptidase 1; VEC, empty vector lentivirus; si, small interfering; oe, overexpression; LMB, leptomycin B.

decreased overall SUMOylation of p27kip1, leading to the increased nuclear and decreased cytoplasmic expression levels of p27kip1, characterized by prominent nuclear retention of p27kip1 (Fig. 5B and C). Consistent with the aforementioned findings, SENP1-oe significantly increased the SUMO level of overall p27kip1 and promoted its cytoplasmic localization and expression. These data demonstrate the role of SENP1 in promoting SUMO1 precursor maturation through hydrolase activity, facilitating p27kip1 SUMOylation within the nucleus.

Additionally, SENP1-C603A, a mutant variant with a cysteine residue substitution at position 603, was used to abolish the isopeptidase activity of SENP1 specifically associated with cytoplasmic deSUMOylation (28,29). SENP1-C603A was successfully transfected into the RBE cells, as demonstrated through western blotting with the FLAG-tag antibody (Fig. 5D). SENP1-C603A reduced nuclear p27kip1 expression levels and increased cytoplasmic expression levels, as determined by western blot and immunofluorescence assays in RBE cells (Fig. 5E and F); consistent with results in SENP1-oe cells. Subsequently, the cytoplasmic protein fraction containing SENP1 was isolated, which was hypothesized to catalyze the deconjugation of SUMO1-substrate complexes to assess the level of p27kip1 deSUMOylation. The deSUMOylated p27kip1 in the cytoplasm of SENP1-C603A cells exhibited notably decreased levels compared with that in SENP1-oe cells; however, this difference was not statistically significant (Fig. 5G). Collectively, these findings suggested that SENP1 may not be involved in regulating the deconjugation process of the p27kip1-SUMO1 complex in cytoplasmic deSUMOylation through its isopeptidase activity.

Knockdown of SENP1 inhibits cell cycle and proliferation by restraining p27kip1 nuclear export in CCA. The aforementioned results demonstrated that SENP1 contributes to the nuclear export of p27kip1. Therefore, the present study aimed to investigate whether the translocation of p27kip1 could lead to changes in CCA phenotypes.

Initially, the interaction levels of CDK2 and cyclin E1 directly bound to p27kip1 in the nucleus were examined. We preserved the conjugation of the proteins with the elution buffer to avoid the heavy chain influence. Decreased interactions of CDK2 and cyclin E1 in SENP1-oe and RBE cells were observed via IP assays, while increased interactions were observed in siSENP1 cells (Fig. 6A). Furthermore, flow cytometry analysis demonstrated that SENP1-oe and SENP1-C603A mutations significantly increased the G_1-S phase transition in RBE cells compared with that in VEC cells (Fig. 6B). In SENP1-oe and SENP1-C603A cells, there was a significant increase in the proportion of cells transitioning from 11.94 and 8.62% in G_1 phase, to 88.06 and 91.38% in S-G_2 phase, respectively, compared with only 22.66 to 77.34% in the VEC cells (Fig. 6B). By contrast, siSENP1 arrested G_1-S phase transition in CCA cells (Fig. 6C). Additionally, SENP1-oe and the SENP1-C603A mutation significantly increased the proliferation of RBE cells, as demonstrated by both CCK-8 and EdU assays. In the CCK-8 experiment, the SENP1-oe and C603A

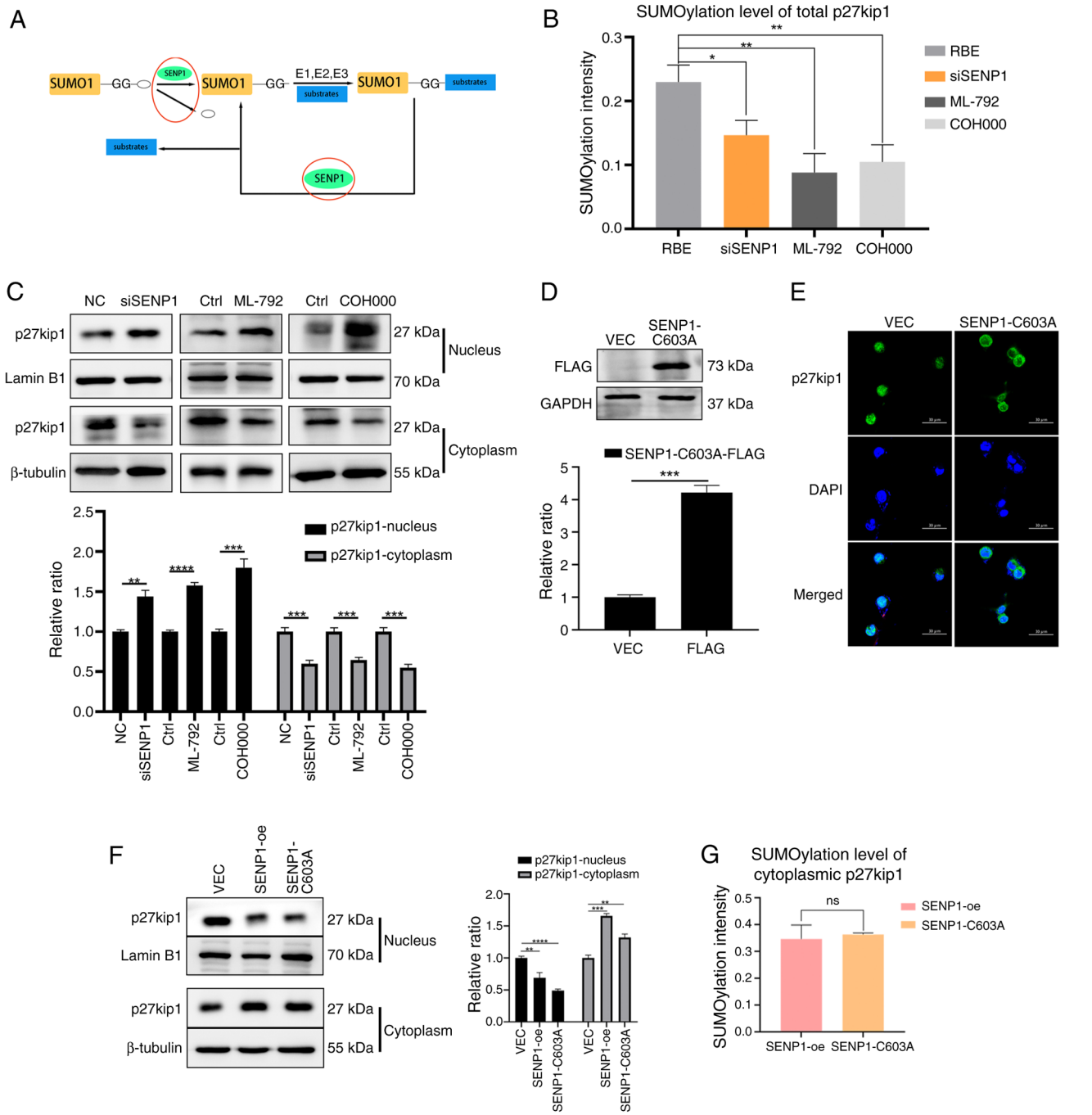

Figure 5. Hydrolase activity of SENP1 serves a crucial role in p27kip1 nuclear export compared with isopeptidase activity. (A) The flow chart shows the full pathway of SUMOylation where the SUMO precursors were firstly hydrolyzed by SENP1 to be matured and subsequently catalyzed by SUMO E1, E2 and E3 to conjugate to the substrates, which were finally deconjugated by SENP1. The red circle shows SENP1 hydrolyzed SUMO precursor and deconjugated SUMO-substrate in the pathway of SUMOylation. (B) ML-792 and COH000-treated RBE cells showed decreased SUMOylation levels of p27kip1 similar to that of siSENP1 cells. (C) ML-792-treated RBE cells showed a similar distribution of p27kip1 between the nucleus and cytoplasm compared with that of siSENP1 cells. (D) Western blot assays showed the SENP1-C603A was successfully transfected in the cells. (E) Immunofluorescence assays showed that SENP1-C603A promoted p27kip1 cytoplasmic retention. (F) Western blot assays showed that SENP1-C603A promoted the p27kip1 nuclear export similar to SENP1-oe cells. (G) Cytoplasmic SUMOylated p27kip1 of SENP1-C603A shows no significant difference compared with SENP1-oe cells. Error bar, mean ± SEM; scale bar, 30 μm; magnification, x100. *P<0.05, **P<0.01, ***P<0.001 and ****P<0.0001. GG, glycine-glycine; ctrl, control; ns, not significant; SENP1, SUMO specific peptidase 1; VEC, empty vector lentivirus; si, small interfering; oe, overexpression.

mutant groups demonstrated faster cell proliferation compared with that of the VEC group (Fig. 6D). Similarly, in the EdU experiment, cell proliferation rates were 64.81 and 62.00% for SENP1 and -C603A mutant groups compared with 43.02% in the VEC group. Conversely, the knockdown of SENP1 decreased proliferation (Fig. 6E). Another CCA cell line, TFK1, was used to verify the phenotype changes caused by the effects of SENP1 expression changes. TFK1 cells showed the same results as the RBE cells: SENP1-oe decreased combinations of CDK2 and cyclin E1 while siSENP1 increased the combinations (Fig. S1A). Flow cytometry analysis demonstrated that SENP1-oe significantly increased the G_1-S phase transition in

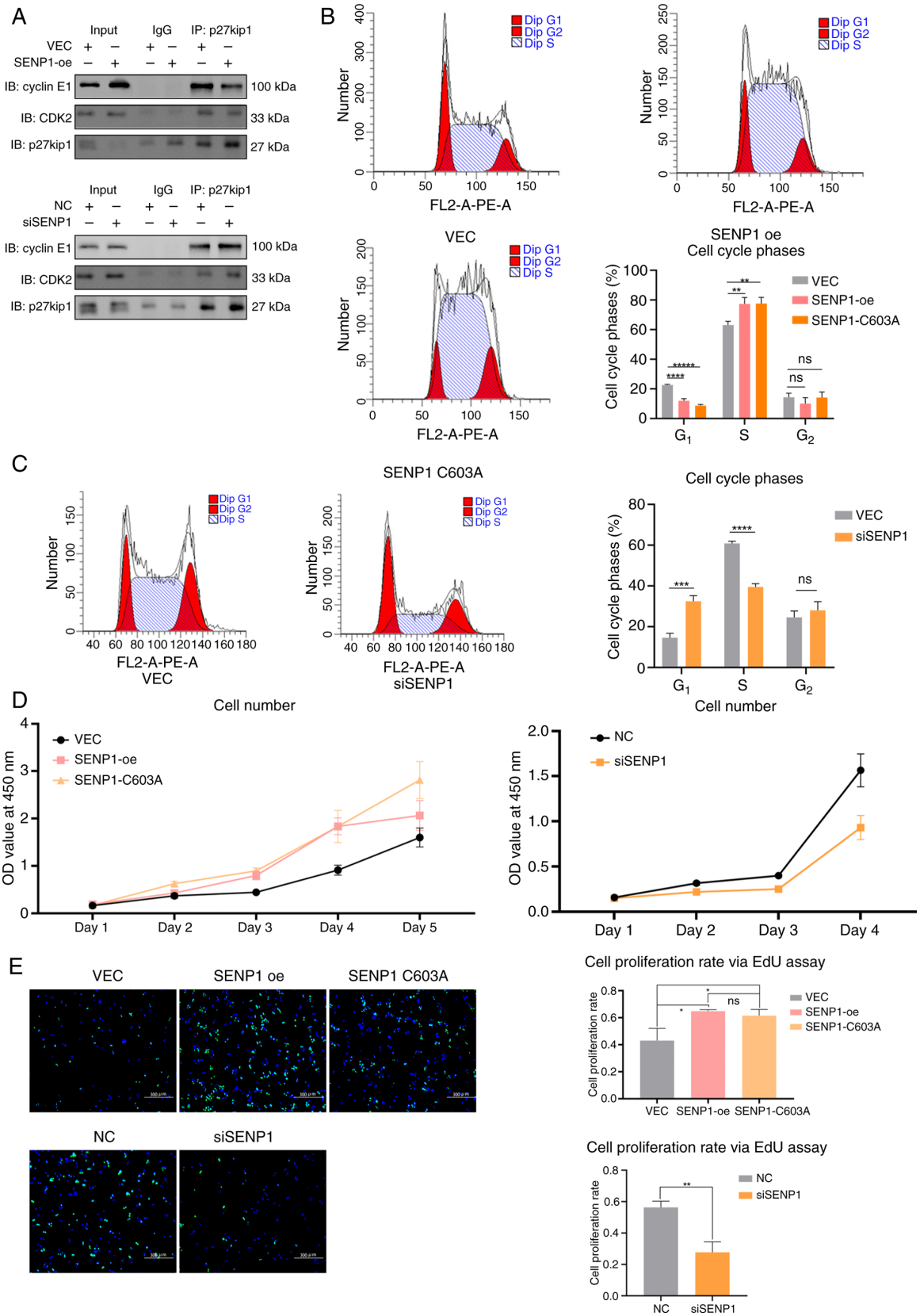

Figure 6. Redistribution of p27kip1 mediated by SENP1-regulated SUMOylation influences the cell cycle and proliferation rates of RBE cells. (A) An IP assay showed SENP1-oe transfection reduced the interactions between p27kip1 and CDK2 or cyclin E1. An IP assay showed SENP1 knockdown promoted interactions between p27kip1 and CDK2 or cyclin E1 in RBE cells. (B) SENP1-oe and -C603A mutation promoted G_1-S phase transition as assessed using flow cytometry analysis in RBE cells. (C) siSENP1 transfection reduced G_1-S phase transition as assessed via flow cytometry analysis in RBE cells. (D) A Cell Counting Kit 8 assay showed that the SENP1-oe and -C603A mutation promoted cell proliferation, while siSENP1 inhibited proliferation of RBE cells. (E) An EdU assay showed SENP1-oe and -C603A mutation increased cell proliferation compared with VEC cells, while siSENP1 decreased proliferation in RBE cells, compared with that in NC cells. Scale bar, 300 μm; magnification, x10. Error bar, mean ± SEM. *P<0.05, **P<0.01, ***P<0.001 and ****P<0.0001. ns, not significant; SENP1, SUMO specific peptidase 1; VEC, empty vector lentivirus; NC, negative control; si, small interfering; oe, overexpression; IB, immunoblotting; IP, immunoprecipitation; EdU, 5-ethynyl-2'-deoxyuridine.

TFK1 cells compared with that in VEC cells, while siSENP1 arrested G_1-S phase transition in TFK1 CCA cells (Fig. S1B). CCK-8 and EdU assays showed that SENP1-oe promoted the cell proliferation of TFK1 cells and siSENP1 suppressed the cell proliferation (Fig. S1C and D).

SENP1-oe and SENP1-C603A exhibited a phenotypic consistency in their impact on cell proliferation and the cell cycle. However, the SENP1-oe and SENP1-C603A cell phenotypes differed significantly from those observed in the SENP1 knockdown group. These findings suggested that the nucleocytoplasmic translocation of p27kip mediated by SENP1 primarily relies on SUMOylation-mediated enhanced nuclear export rather than the deconjugation process of the p27kip1-SUMO1 complexes through cytoplasmic deSUMOylation. Consequently, SENP1 significantly influences the progression of the CCA cell cycle and cell proliferation; therefore, inhibiting SENP1 may potentially impede cell cycle progression and proliferation in CCA.

Knockdown of SENP1 increases the chemosensitivity of cis-platinum by restraining nuclear export of p27kip1 in CCA. Cis-platinum administration is crucial in the standard management of unresectable CCA and is widely recognized as the most efficacious first-line therapeutic regimen (30-32). The present study investigated whether the translocation of p27kip1 induced by SENP1 contributes to cis-platinum resistance in CCA chemotherapy (Fig. 7). First, the survival rate of RBE cells against cis-platinum was analyzed and the IC_{50} value was determined for cis-platinum. A marked decreased IC_{50} value of cis-platinum was demonstrated in SENP1-knockdown CCA cells compared with that in untreated cells. In comparison, a markedly increased IC_{50} value was observed in SENP1-oe cells compared with that in the RBE group (Fig. 7A). Western blot analysis demonstrated that SENP1-oe was associated with significantly increased expression levels of chemotherapy resistance-associated proteins MDR1 and MRP1 compared with that in the VEC group (Fig. 7B). Upon treatment with 4 μM cis-platinum treatment, SENP1-oe resulted in significant inhibition of apoptosis, leading to a decrease in the apoptotic rate from 37.53% in the control group to 15.48% in the group, with elevated levels of SENP1 expression. Simultaneously, the expression levels of the pro-apoptotic protein Bax decreased by 45.1% in the SENP1-oe group and 62.2% in the SENP1-C603A cells compared with that in the VEC cells, while the anti-apoptotic protein Bcl-2 increased to 2.18-fold in the SENP1-oe group and 1.85-fold in the SENP1-C603A cells compared with that in the VEC cells. The ratio of cleaved caspase-3/caspase-3 expression was decreased by 24.5 and 74.0% in SENP1-oe and SENP1-C603A cells, respectively, compared with that in the VEC group (Fig. 7C). Concurrently, the siSENP1 group showed significantly decreased expression levels of MDR1 and MRP1 compared with that in the NC group (Fig. 7D). The pro-apoptotic protein Bax increased to 4.56- and 3.50-fold in the siSENP1 groups compared with that of the NC group. The anti-apoptotic protein Bcl-2 expression levels showed a 73.5 and 73.7% decline in the two siSENP1 cells compared with that in the NC cells. The ratio of cleaved caspase-3/caspase-3 increased by 179 and 190% in the two siSENP1 cells compared with that in the NC cells (Fig. 7E) SENP1 knockdown promoted apoptosis, significantly increasing the apoptotic rate to 88.30% (Fig. 7F). The same assays were conducted using the TFK1 cell line, which showed the same results as aforementioned (Fig. S2), suggesting that SENP1-oe increased the IC_{50} value of cis-platinum, and decreased the expression of MDR1, MRP1, pro-apoptotic protein Bax and the ratio of cleaved caspase-3/caspase-3, but increased the anti-apoptotic protein Bcl-2 expression (Fig. S2A-C). The siSENP1-treated TFK1 cells showed a lower IC_{50} value of cis-platinum, and increased expression of MDR1, MRP1, pro-apoptotic protein Bax and the ratio of cleaved caspase-3/caspase-3, while the anti-apoptotic protein Bcl-2 expression decreased (Fig. S2A, D and E). These results suggested that SENP1 knockdown increased the sensitivity of CCA cells to cis-platinum, potentially by decreasing the nuclear export of p27kip1.

Discussion

A critical mechanism underlying tumorigenesis and cancer chemotherapy resistance is the aberrant subcellular localization of drug targets or tumor suppressors, such as p53, PTEN, deleted in liver cancer-1 and Wilms tumor gene on the X chromosome (33-36). As a tumor suppressor, p27kip1 typically resides in the nucleus, where it binds to CDK-cyclins to halt cell cycle progression from G_1 to S phase, subsequently influencing cell proliferation and apoptosis (3,4). However, cytoplasmic mislocalization of p27kip1 has been associated with unfavorable clinical prognosis and drug resistance in various types of cancer, including CCA (37,38). The present study demonstrated that SUMOylation is pivotal in the aberrant cytoplasmic localization of p27kip1 in CCA (13,14). SENP1 regulates the reversible process of protein covalent modification by SUMO1, which is involved in SUMOylation and/or deSUMOylation and is frequently upregulated in cancer types, such as lung, head and neck, colorectal and prostate cancer (3,4,39). However, the current understanding of the impact of SENP1 on the cytoplasmic localization of p27kip1 in CCA remains limited.

Through analysis of TCGA data across a pan-cancer panel, the present study substantiated that a large proportion of malignant tumors (18 out of 33 types of cancer analyzed) exhibited a significant upregulation of SENP1 expression levels, thereby demonstrating that SENP1 may serve a pivotal role in tumorigenesis. Furthermore, upregulated expression levels of SENP1 demonstrated notable associations with tumor stage and poor lymph node metastasis in CCA, based on data from the TCGA database and CCA tumor samples analyzed. These results suggested that increased expression levels of SENP1 may also potentially contribute to CCA pathogenesis and progression. Additionally, there was a significant correlation between SENP1 and p27kip1. Therefore, it was considered that the positive correlation may be dependent upon the interplay between SENP1 and cytoplasmic p27kip1. As with our previous study (14), there was an increase in p27kip1 expression transitioning from nuclear to cytoplasmic localization as the TNM stages progressed. These results were further confirmed through immunofluorescence assays to visualize the nuclear-cytoplasmic translocation, conducted on the CCA cell line.

SENP1 possesses two enzymatic activities: Isopeptidase and hydrolase. Isopeptidase activity deconjugates SUMO1

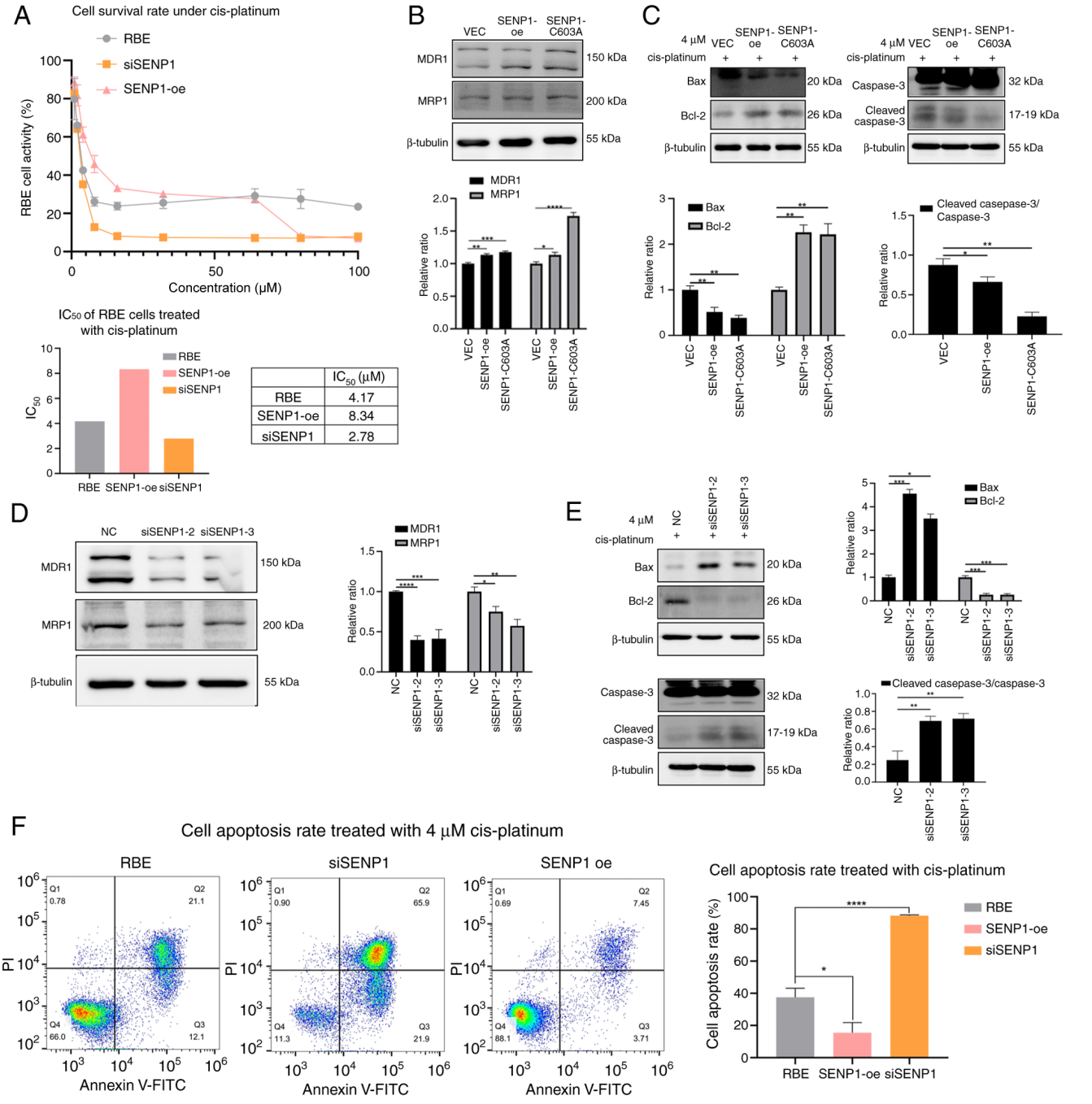

Figure 7. Redistribution of p27kip1 mediated by SENP1-regulated SUMOylation affects chemotherapy resistance in RBE cells. (A) The IC_{50} of RBE cells against cis-platinum was reduced in siSENP1 cells, while SENP1-oe cells increased the IC_{50} of RBE cells against cis-platinum, compared with that of VEC cells (B) SENP1-oe and -C603A cells showed increased expression levels of chemotherapy resistance-associated proteins MDR1 and MRP1. (C) SENP1-oe and -C603A cells showed decreased expression levels of apoptotic proteins Bax and cleaved caspase-3 (normalized to caspase-3), and increased expression levels of anti-apoptotic protein Bcl-2, with 4 μM cis-platinum treatment. (D) siSENP1 cells showed decreased expression of chemotherapy resistance-associated proteins MDR1 and MRP1. (E) siSENP1 cells showed increased expression levels of apoptotic proteins Bax and cleaved caspase-3 (normalized to caspase-3), and decreased expression levels of anti-apoptotic protein Bcl-2 under 4 μM cis-platinum. (F) siSENP1 cells showed an increased apoptotic rate with 4 μM cis-platinum treatment analyzed by flow cytometry, and SENP1-oe cells showed a decreased apoptotic rate compared with that of NC cells. Error bar, mean ± SEM. *P<0.05, **P<0.01, ***P<0.001 and ****P<0.0001. SENP1, SUMO specific peptidase 1; VEC, empty vector lentivirus; NC, negative control; si, small interfering; oe, overexpression; MDR1, multidrug resistance 1; MRP1, multidrug resistance-associated protein 1.

from the target protein lysine residue, and hydrolase activity processes SUMO1 precursor by exposing the C-terminal diglycine residue, which is activated by the E1 enzyme. The activated SUMO1 is transferred to UBE2I and eventually covalently attaches to lysine residues of substrates by SUMO E3 enzymes (40,41). ML-792 and COH000, specific SUMO E1 activating enzyme inhibitors, were used to inhibit the hydrolase activity pathway of SENP1 involved in nuclear SUMOylation. The inhibitors restricted p27kip1 in the nucleus, similar to the SENP1 knockdown, demonstrating the importance of hydrolase activity of SENP1 in p27kip1 translocation.

Additionally, SENP1-C603A was utilized to effectively suppress the isopeptidase activity of SENP1, which is related explicitly to cytoplasmic deSUMOylation. The

present findings indicated that SENP1 primarily demonstrated C-terminal hydrolase activity, thereby increasing the level of SUMO modification on p27kip1 and promoting its cytoplasmic localization by facilitating the maturation of SUMO1 precursor. Furthermore, SENP1 serves a minor role in the deSUMOylation of p27kip1 in the cytoplasm. However, other studies have reported that isopeptidase activity is crucial in regulating JAK2, homeodomain-interacting protein kinase 1 and glioma-associated oncogene homolog 1 translocation (17,21,24,42). Therefore, it could be suggested that the exact function of SENP1 may also be associated with its substrate specificity. In addition, the dissociation of the SUMO1-p27kip1 complex within the cytoplasm may potentially be facilitated by other SENPs, such as SENP2 and desumoylating isopeptidase 1 (43-45). However, further confirmation is required to validate this hypothesis.

The presence of SENP1 is essential for ensuring the proper assembly and function of nuclear pore complexes (NPCs), facilitating their appropriate localization and translocation activity (8). To further elucidate whether the cytoplasmic localization of p27kip1 induced by SENP1 is attributed to an augmented nuclear export of p27kip1 mediated by enhanced SUMOylation, LMB, a specific inhibitor of CRM1, was used to specifically inhibit the nuclear export of p27kip1. In agreement with the aforementioned findings, the specific role SENP1 in expediting the maturation of SUMO1 precursor, facilitating p27kip1 SUMOylation and promoting nuclear export of p27kip1, was further substantiated. Consequently, it could be suggested that the predominant nuclear localization of SENP1 and its role as a component of NPCs are crucial for its hydrolase activity, rather than the isopeptidase function of SENP1, which facilitates p27kip1 SUMOylation and specifically promotes its nuclear export process.

The impact of SENP1 on the functionality and phenotypic characteristics of p27kip1 was further investigated through both overexpression and knockdown experiments. Overexpression of SENP1 increased p27kip1 interactions with CDK2-cyclin E1, promoted the G_1-S phase cell cycle transition and increased the CCA cell proliferation. Conversely, these effects were reversed when SENP1 was knocked down by siRNA. Additionally, the knockdown of SENP1 significantly increased the chemosensitivity of the CCA cell line to cis-platinum compared with that of the control group and SENP1-oe cells. These findings suggested that SENP1 serves a vital role in regulating p27kip1 function.

Future studies may include investigation of the deSUMOylation enzymes of p27kip1 and upstream signaling of SUMOylation regulation across various tissues, such as those that are rarely cured following cancerization, such as pancreatic or bile duct tissues. An animal study will be an important step in the investigation of SUMOylation upstream regulation. Mouse models could be generated with upregulated SENP1, SUMO1, UBE2I and RNF4 expression, respectively, to avoid the death of embryos resulting from knockdown of some of the genes. Next, the whole genome and proteome could be detected via sequencing analysis and mass spectrum analysis using the bile duct tissue to determine the upstream regulation of SUMOylation in the bile duct. In conclusion, to the best of our knowledge, the present study is the first to demonstrate the key role of SENP1 hydrolase activity in enhancing the SUMO modification of p27kip1 and promoting p27kip1 cytoplasmic translocation by facilitating SUMO1 precursor maturation. This mechanism highlights the potential involvement of SENP1 and SUMOylation in p27kip1 nuclear export, which provides a potential novel therapeutic target for CCA treatment in the future.

Acknowledgements

Not applicable.

Funding

The present study was supported by the National Natural Science Fund (grant no. 8167101526) and the Natural Science Foundation of Hubei Province (grant no. 2019CFB653).

Availability of data and materials

The data generated in the present study may be requested from the corresponding author.

Authors' contributions

KJ performed study conceptualization, methodology, software analysis, formal results analysis, investigation, data curation, original draft writing, manuscript review and editing, visualization and project administration. WY undertook original draft writing, formal analysis and data curation. JH performed manuscript review and editing, methodology, software analysis and formal analysis. XT and YL performed manuscript review and editing, surgical investigations and acquired clinical sample resources. ST undertook original draft writing and analysis of experimental results using software. JL was responsible for study conceptualization, acquiring resources, manuscript review and editing, project administration, supervision and funding acquisition. All authors read and approved the final manuscript. KJ and JL confirm the authenticity of all the raw data.

Ethics approval and consent to participate

All procedures performed involving human participants were in accordance with the ethical standards of the institutional and/or national research committee and with the 1964 Helsinki declaration and its later amendments or comparable ethical standards. All study procedures were approved by the Ethics Committee of Tongji Hospital, Huazhong University of Science and Technology (Wuhan, China; approval no. TJ-IRB202502103). Patients included in the present study have provided informed written to participate.

Patient consent for publication

Not applicable.

Competing interests

The authors declare that they have no competing interests.

References

1. Banales JM, Marin JJG, Lamarca A, Rodrigues PM, Khan SA, Roberts LR, Cardinale V, Carpino G, Andersen JB, Braconi C, *et al*: Cholangiocarcinoma 2020: The next horizon in mechanisms and management. Nat Rev Gastroenterol Hepatol 17: 557-588, 2020.
2. Darwish Murad S, Kim WR, Harnois DM, Douglas DD, Burton J, Kulik LM, Botha JF, Mezrich JD, Chapman WC, Schwartz JJ, *et al*: Efficacy of neoadjuvant chemoradiation, followed by liver transplantation, for perihilar cholangiocarcinoma at 12 US centers. Gastroenterology 143: 88-98.e3, e14, 2012.
3. Chu IM, Hengst L and Slingerland JM: The Cdk inhibitor p27 in human cancer: Prognostic potential and relevance to anticancer therapy. Nat Rev Cancer 8: 253-267, 2008.
4. Razavipour SF, Harikumar KB and Slingerland JM: p27 as a transcriptional regulator: New roles in development and cancer. Cancer Res 80: 3451-3458, 2020.
5. Jeannot P, Nowosad A, Perchey RT, Callot C, Bennana E, Katsube T, Mayeux P, Guillonneau F, Manenti S and Besson A: $p27^{Kip1}$ promotes invadopodia turnover and invasion through the regulation of the PAK1/Cortactin pathway. Elife 6: e22207, 2017.
6. Li N, Zeng J, Sun F, Tong X, Meng G, Wu C, Ding X, Liu L, Han M, Lu C and Dai F: p27 inhibits CDK6/CCND1 complex formation resulting in cell cycle arrest and inhibition of cell proliferation. Cell Cycle 17: 2335-2348, 2018.
7. McKay LK and White JP: The AMPK/$p27^{Kip1}$ pathway as a novel target to promote autophagy and resilience in aged cells. Cells 10: 1430, 2021.
8. Chang HM and Yeh ETH: SUMO: From bench to bedside. Physiol Rev 100: 1599-1619, 2020.
9. Flotho A and Melchior F: Sumoylation: A regulatory protein modification in health and disease. Annu Rev Biochem 82: 357-385, 2013.
10. Vertegaal AC: SUMO chains: Polymeric signals. Biochem Soc Trans 38: 46-49, 2010.
11. Tokarz P and Woźniak K: SENP proteases as potential targets for cancer therapy. Cancers (Basel) 13: 2059, 2021.
12. Kunz K, Piller T and Müller S: SUMO-specific proteases and isopeptidases of the SENP family at a glance. J Cell Sci 131: jcs211904, 2018.
13. Yang J, Liu Y, Wang B, Lan H, Liu Y, Chen F, Zhang J and Luo J: Sumoylation in p27kip1 via RanBP2 promotes cancer cell growth in cholangiocarcinoma cell line QBC939. BMC Mol Biol 18: 23, 2017.
14. Huang J, Tan X, Liu Y, Jiang K and Luo J: Knockdown of UBE2I inhibits tumorigenesis and enhances chemosensitivity of cholangiocarcinoma via modulating p27kip1 nuclear export. Mol Carcinog 62: 700-715, 2023.
15. Cheng J, Kang X, Zhang S and Yeh ET: SUMO-specific protease 1 is essential for stabilization of HIF1alpha during hypoxia. Cell 131: 584-595, 2007.
16. Gao Y, Wang R, Liu J, Zhao K, Qian X, He X and Liu H: SENP1 promotes triple-negative breast cancer invasion and metastasis via enhancing CSN5 transcription mediated by GATA1 deSUMOylation. Int J Biol Sci 18: 2186-2201, 2022.
17. Li J, Wu R, Yung MMH, Sun J, Li Z, Yang H, Zhang Y, Liu SS, Cheung ANY, Ngan HYS, *et al*: SENP1-mediated deSUMOylation of JAK2 regulates its kinase activity and platinum drug resistance. Cell Death Dis 12: 341, 2021.
18. Zhu S, Hu J, Cui Y, Liang S, Gao X, Zhang J and Jia W: Knockdown of SENP1 inhibits HIF-1α SUMOylation and suppresses oncogenic CCNE1 in Wilms tumor. Mol Ther Oncolytics 23: 355-366, 2021.
19. Amin MB, Edge S, Greene F, Byrd DR, Brookland RK, Washington MK, *et al*: AJCC Cancer Staging Manual. Vol 22. 8th edition. Springer International Publishing: American Joint Commission on Cancer, Chicago, pp287-293, 2017.
20. Chandrashekar DS, Karthikeyan SK, Korla PK, Patel H, Shovon AR, Athar M, Netto GJ, Qin ZS, Kumar S, Manne U, *et al*: UALCAN: An update to the integrated cancer data analysis platform. Neoplasia 25: 18-27, 2022.
21. Chandrashekar DS, Bashel B, Balasubramanya SAH, Creighton CJ, Rodriguez IP, Chakravarthi BVSK and Varambally S: UALCAN: A portal for facilitating tumor subgroup gene expression and survival analyses. Neoplasia 19: 649-658, 2017.
22. Li C, Tang Z, Zhang W, Ye Z and Liu F: GEPIA2021: Integrating multiple deconvolution-based analysis into GEPIA. Nucleic Acids Res 49: W242-W246, 2021.
23. Specht E, Kaemmerer D, Sänger J, Wirtz RM, Schulz S and Lupp A: Comparison of immunoreactive score, HER2/neu score and H score for the immunohistochemical evaluation of somatostatin receptors in bronchopulmonary neuroendocrine neoplasms. Histopathology 67: 368-377, 2015.
24. Li X, Luo Y, Yu L, Lin Y, Luo D, Zhang H, He Y, Kim YO, Kim Y, Tang S and Min W: SENP1 mediates TNF-induced desumoylation and cytoplasmic translocation of HIPK1 to enhance ASK1-dependent apoptosis. Cell Death Differ 15: 739-750, 2008.
25. Wang Y, Wang Y, Xiang J, Ji F, Deng Y, Tang C, Yang S, Xi Q, Liu R and Di W: Knockdown of CRM1 inhibits the nuclear export of p27(Kip1) phosphorylated at serine 10 and plays a role in the pathogenesis of epithelial ovarian cancer. Cancer Lett 343: 6-13, 2014.
26. Connor MK, Kotchetkov R, Cariou S, Resch A, Lupetti R, Beniston RG, Melchior F, Hengst L and Slingerland JM: CRM1/Ran-mediated nuclear export of p27(Kip1) involves a nuclear export signal and links p27 export and proteolysis. Mol Biol Cell 14: 201-213, 2003.
27. He X, Riceberg J, Soucy T, Koenig E, Minissale J, Gallery M, Bernard H, Yang X, Liao H, Rabino C, *et al*: Probing the roles of SUMOylation in cancer cell biology by using a selective SAE inhibitor. Nat Chem Biol 13: 1164-1171, 2017.
28. Xu Z, Chau SF, Lam KH, Chan HY, Ng TB and Au SWN: Crystal structure of the SENP1 mutant C603S-SUMO complex reveals the hydrolytic mechanism of SUMO-specific protease. Biochem J 398: 345-352, 2006.
29. Xu Z and Au SWN: Mapping residues of SUMO precursors essential in differential maturation by SUMO-specific protease, SENP1. Biochem J 386: 325-330, 2005.
30. Elvevi A, Laffusa A, Scaravaglio M, Rossi RE, Longarini R, Stagno AM, Cristoferi L, Ciaccio A, Cortinovis DL, Invernizzi P and Massironi S: Clinical treatment of cholangiocarcinoma: An updated comprehensive review. Ann Hepatol 27: 100737, 2022.
31. Li Y, Song Y and Liu S: The new insight of treatment in cholangiocarcinoma. J Cancer 13: 450-464, 2022.
32. Macias RIR, Rimassa L and Lamarca A: The promise of precision medicine: How biomarkers are shaping the future of cholangiocarcinoma treatment. Hepatobiliary Surg Nutr 12: 457-461, 2023.
33. Yuan J, Luo K, Zhang L, Cheville JC and Lou Z: USP10 regulates p53 localization and stability by deubiquitinating p53. Cell 140: 384-396, 2010.
34. Chen JH, Zhang P, Chen WD, Li DD, Wu XQ, Deng R, Jiao L, Li X, Ji J, Feng GK, *et al*: ATM-mediated PTEN phosphorylation promotes PTEN nuclear translocation and autophagy in response to DNA-damaging agents in cancer cells. Autophagy 11: 239-252, 2015.
35. Yuan BZ, Jefferson AM, Millecchia L, Popescu NC and Reynolds SH: Morphological changes and nuclear translocation of DLC1 tumor suppressor protein precede apoptosis in human non-small cell lung carcinoma cells. Exp Cell Res 313: 3868-3880, 2007.
36. Rivera MN, Kim WJ, Wells J, Stone A, Burger A, Coffman EJ, Zhang J and Haber DA: The tumor suppressor WTX shuttles to the nucleus and modulates WT1 activity. Proc Natl Acad Sci USA 106: 8338-8343, 2009.
37. Luo J, Chen Y, Li Q, Wang B, Zhou Y and Lan H: CRM-1 knockdown inhibits extrahepatic cholangiocarcinoma tumor growth by blocking the nuclear export of p27Kip1. Int J Mol Med 38: 381-390, 2016.
38. Lee J and Kim SS: The function of p27 KIP1 during tumor development. Exp Mol Med 41: 765-771, 2009.
39. Burdelski C, Menan D, Tsourlakis MC, Kluth M, Hube-Magg C, Melling N, Minner S, Koop C, Graefen M, Heinzer H, *et al*: The prognostic value of SUMO1/Sentrin specific peptidase 1 (SENP1) in prostate cancer is limited to ERG-fusion positive tumors lacking PTEN deletion. BMC Cancer 15: 538, 2015.
40. Hay RT: SUMO: A history of modification. Mol Cell 18: 1-12, 2005.
41. Palancade B and Doye V: Sumoylating and desumoylating enzymes at nuclear pores: Underpinning their unexpected duties? Trends Cell Biol 18: 174-183, 2008.
42. Liu H, Yan S, Ding J, Yu TT and Cheng SY: DeSUMOylation of gli1 by SENP1 attenuates sonic hedgehog signaling. Mol Cell Biol 37: e00579-16, 2017.
43. Hang J and Dasso M: Association of the human SUMO1 protease SENP2 with the nuclear pore. J Biol Chem 277: 19961-19966, 2002.
44. Ball JR and Ullman KS: Versatility at the nuclear pore complex: Lessons learned from the nucleoporin Nup153. Chromosoma 114: 319-330, 2005.
45. Shin EJ, Shin HM, Nam E, Kim WS, Kim JH, Oh BH and Yun Y: DeSUMOylating isopeptidase: A second class of SUMO protease. EMBO Rep 13: 339-346, 2012.